# Cluster-beam deposition of thin metallic antimony films: Cluster-size and deposition-rate effects

G. Fuchs, P. Melinon, F. Santos Aires, M. Treilleux, B. Cabaud, and A. Hoareau
*Département de Physique des Matériaux, Université Claude Bernard-Lyon I,*
*43 Boulevard du 11 Novembre 1918, 69622 Villeurbanne CEDEX, France*
(Received 29 January 1991)

Low-energy cluster-beam deposition is a technique that allows the growth of thin films via a mechanism different from the conventional molecular-beam deposition technique. These differences have been recently demonstrated in the case of antimony. This work shows that the deposition rate and the mean size of incident clusters of Sb evaporated on amorphous carbon are two crucial parameters. Crystalline aspect and coverage rate of deposits depends strongly on these two parameters. Transmission-electron-microscopy studies allow us to determine the optimum conditions under which, especially in the case of low-energy cluster-beam deposition, very thin films of high quality may be obtained.

## I. INTRODUCTION

Recent advances in the technology of thin-film deposition have allowed the growth of high-quality (well-crystallized and continuous) and reproducible thin films. The growth of reproducible high-quality films has led to numerous recent advances in thin-film deposition technology. In many microelectronic devices, elements of column VB (P, As, Sb) in the Periodic Table are used in the formation of components (III-V semiconductors, superlattices, superconductor devices). Among these materials, the case of antimony has been extensively studied.[1-3] The elements of column IIIB evaporate as atoms while those of column VB are known to evaporate as molecular structures (tetrameric form for antimony, arsenic, and phosphorous.[4] It is well known that the process leading to the growth of high-quality films (thin continuous films, stoichiometric composition, etc.) is difficult to control. Consequently, a deposition technique using low-energy clusters is proposed as a solution to these problems and is reported here.

Recent studies[5,6] have shown that differences between low-energy cluster-beam deposition (LECBD) and molecular-beam deposition (MBD) exist. It has been pointed out[5] that, in the first stages of antimony deposition, these low-energy clusters (48 atoms mean size) tend to form deposits which are significantly different from the ones obtained from molecular-vapor deposition (tetrameric $Sb_4$).

The work deals, on the one hand, with the presentation of experimental results demonstrating the influence of the cluster size (from 16 to 240 atoms) and the deposition rate on the growth mechanism of antimony deposits obtained with LECBD. On the other hand, these results allow us to determine the best conditions to obtain high-quality thin films and to present a tentative description of the growth mechanism in the case of LECBD. The dependence of the diffusion coefficient on the *a*-C substrate as a function of the number of atoms per incident cluster is discussed.

## II. EXPERIMENTAL PROCEDURE

The cluster beam is generated by the gas aggregation technique in a source similar to that developed by Sattler.[7] The metallic vapor coming from a heated crucible condenses in an inert gas (helium or argon) cooled at liquid-nitrogen temperature. The cluster size is monitored by the helium pressure for the smaller ones (up to 100 atoms), and by argon pressure for the larger ones (from 100 to 500 atoms). In the case of helium, experimental results show that the increase of inert gas pressure induces a decrease of cluster size.[8] A time-of-flight mass spectrometer is used in order to measure the cluster-size distribution before the deposition. For low masses, previous results on fragmentation[9] lead us to believe that ionized cluster mass distribution is a good measure of the neutral cluster distribution. On the other hand, no mass discrimination has been detected for large masses ($n > 500$, where $n$ is the number of atoms per cluster) by varying the nature and pressure of the inert gas. Further experimental details have been published previously.[10] The experimental cluster-size distribution may be approximated by a Gaussian law: mean cluster size $\langle n \rangle$ and dispersion $\sigma$ are $(\langle n \rangle, \sigma)=(16,12)$, (36,28), and (240,240). The typical size distribution is given in Fig. 1. The size of the clusters will be identified as the mean size in the following discussion.

These neutral clusters are deposited at room temperature on amorphous carbon films (5 nm thickness) supported on copper microscopy grids. The MBD experiment was performed in the same oven in absence of cold helium gas. In this configuration, antimony vapor is formed essentially with $Sb_4$. The residual pressure is less than $10^{-4}$ Pa. In order to prevent any air contamination of the deposit, a thin carbon film of 5 nm has been evaporated *in situ* after the antimony deposition. During the antimony evaporation, the deposited thickness $d$ and the rate of deposition $R$ are controlled by a crystal quartz rate monitor located near the substrates. The fluctuation in the deposition rate was lower than 10% for the max-

 

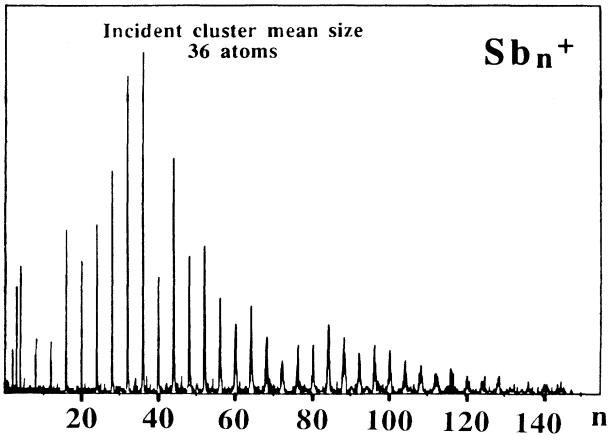


FIG. 1. Typical size distribution of ionized antimony clusters obtained with an incident mean cluster size of 36 atoms. The electron energy used to ionize the antimony clusters is about 20 eV.

imum time of exposure. To control the desorption rate on the substrate, the thickness of the deposit is checked using the RBS technique (Rutherford backscattering spectrometry). The deposition rate is fixed at $5\times10^{-3}$ nm s$^{-1}$ for the study of the cluster-size effect. For the study of the diffusion effect, the deposition rate was studied in the range from $3\times10^{-2}$ to $1.7\times10^{-1}$ nm s$^{-1}$ which corresponds to a mean cluster impinging the flux of $2.8\times10^{12}$ clusters to $1.6\times10^{13}$ clusters cm$^{-2}$s$^{-1}$ for MBD and LECBD ($Sb_{36}$ deposition).

## III. RESULTS

### A. Influence of incident cluster mean size on the film growth

The evolution of antimony thin-film growth versus incident cluster size is presented in Fig. 2. Figures 2(a)–2(d) correspond to 1 nm thickness and Figs. 2(e)–2(h) to 5 nm thickness. For each thickness, the evaporation rate remains constant while the incident cluster size increases

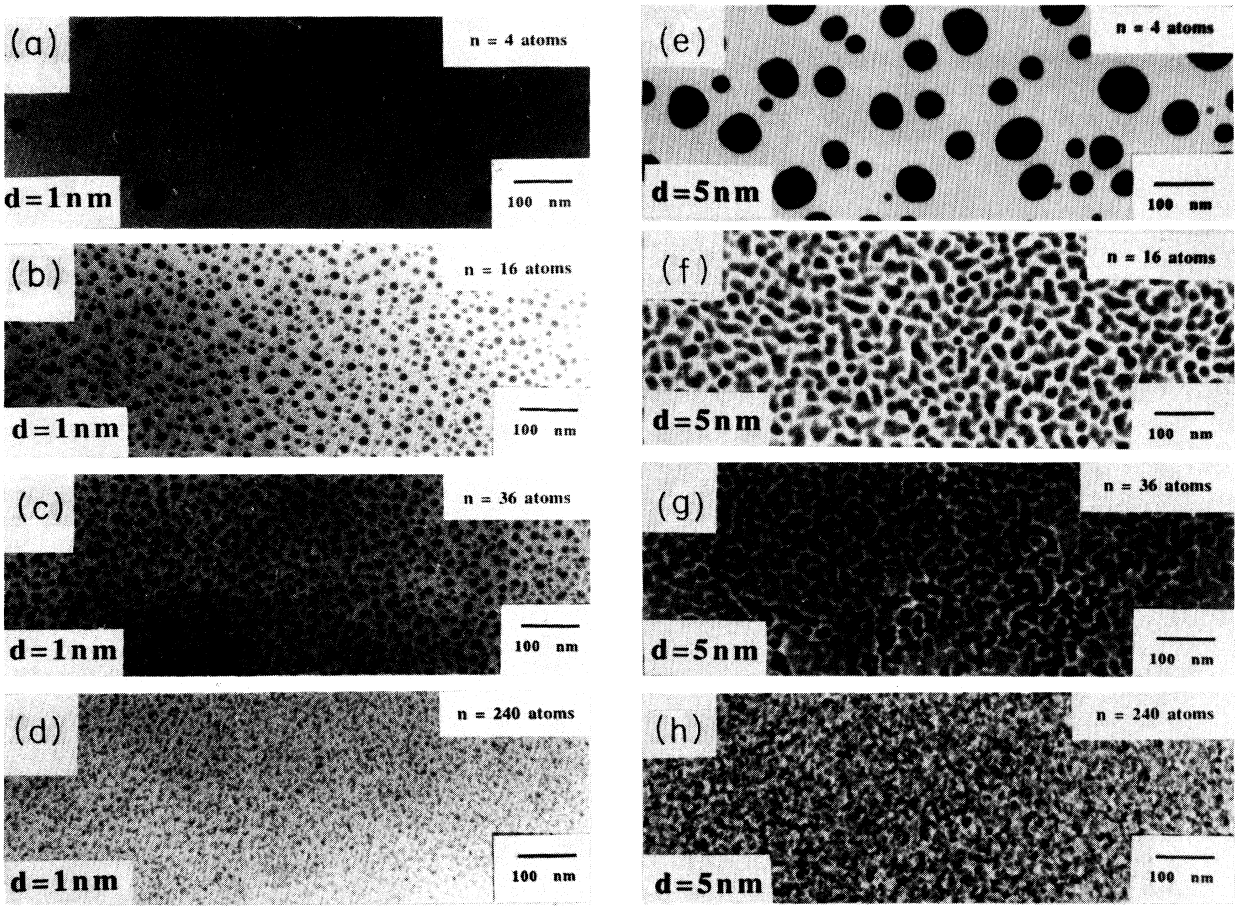


FIG. 2. TEM micrographs of 1-nm- (a)–(d) and 5-nm-thick antimony deposits (e)–(h) obtained with increasing incident mean cluster size: (a) and (e) $N=4$ atoms (MBD), (b) and (f) $N=16$ atoms, (c) and (g) $N=36$ atoms, and (d) and (h) $N=240$ atoms. The deposition rate is fixed at $5\times10^{-3}$ nm s$^{-1}$.

TABLE I. Evolution of the mean diameter ($D$) and number of supported antimony particles per square centimeter ($N_s$) experimentally measured on a 1-nm-thick deposit for various incident cluster size. $\langle n \rangle$ represents the mean number of atoms in the incident cluster.

| $\langle n \rangle$ atoms | 4 | 16 | 36 | 240 |
|---|---|---|---|---|
| D (nm) | 27.8 | 11.5 | 10.2 | a |
| $N_s$ | $0.44\times10^{10}$ | $28\times10^{10}$ | $36.5\times10^{10}$ | a |

[a]For high values of $n$, coalescence prevents any determination of $D$ and $N_s$.

from $\langle n \rangle = 4$ atoms (MBD) to 240 atoms in the LECBD configuration. For both thicknesses, incident cluster size has an influence on the mechanism of the film growth. Large differences in the nucleation density and nuclei size appear between molecular deposition [Figs. 2(a) and 2(e)] and small cluster deposition [$\langle n \rangle = 16$ atoms, Figs. 2(b) and 2(f)]. This size effect is still more significant when the incident cluster size increases from $\langle n \rangle = 16$ to 240 atoms [Figs. 2(c), 2(d) and 2(f)–2(h)].

The tetramer deposition gives no continuous layer up to a thickness of 5 nm [Fig. 2(e)]. In this case, the deposit is formed with large clusters randomly distributed on the amorphous carbon substrate. The mean size calculated on large collections of particles is about 28 nm for the 1-nm thick deposit and 41 nm for the 5 nm-thick one. The number density of supported particles increases from $4\times10^9$ cm$^{-2}$ (1 nm thickness) to $2\times10^{10}$ cm$^{-2}$ (5 nm thickness). A decrease of the mean size is observed for the LECBD deposits [Figs. 2(b)–2(d) and 2(f)–2(h)] compared with MBD. At the same time, the increase of incident cluster mean size induces an increase of the particle density as shown in Table I. Hence, for a given thickness, the coverage rate increases with the incident cluster mean size and the deposit tends to be more continuous. In the range of the incident cluster size, this phenomenon has been always observed in our experiments.

### B. Influence of the deposition rate on the growth of antimony film

In the case of MBD, the influence of the deposition rate on the growth of antimony deposit is well known.[11] The increase of deposition rate induces a decrease of the supported particle size together with a better coverage rate.[11] Assuming that incident particles diffuse on the substrate before they become trapped on preferential sites (which are the nucleations centers), the measurement of the saturation embryos number ($N_s$) gives some information on the number of preferential sites on the $a$-C substrate. The deposition rate $R$ must be low to promote nucleation on these preferential sites (P.S.). The study of $N_s$ versus the thickness gives a number density of preferential sites equal to $1.6\times10^{10}$ cm$^{-2}$ ($R = 5\times10^{-3}$ nm s$^{-1}$) which is in good agreement with literature results [$2\times10^{10}$ cm$^{-2}$ (Ref. 12)].

In the case of a deposition of Sb by LECBD (where the mean size of clusters is 36 atoms), the evolution of antimony film growth versus deposition rate can be illustrated by the micrographs of Figs. 3(a)–3(d). The thickness of deposits obtained by the LECBD technique is 10

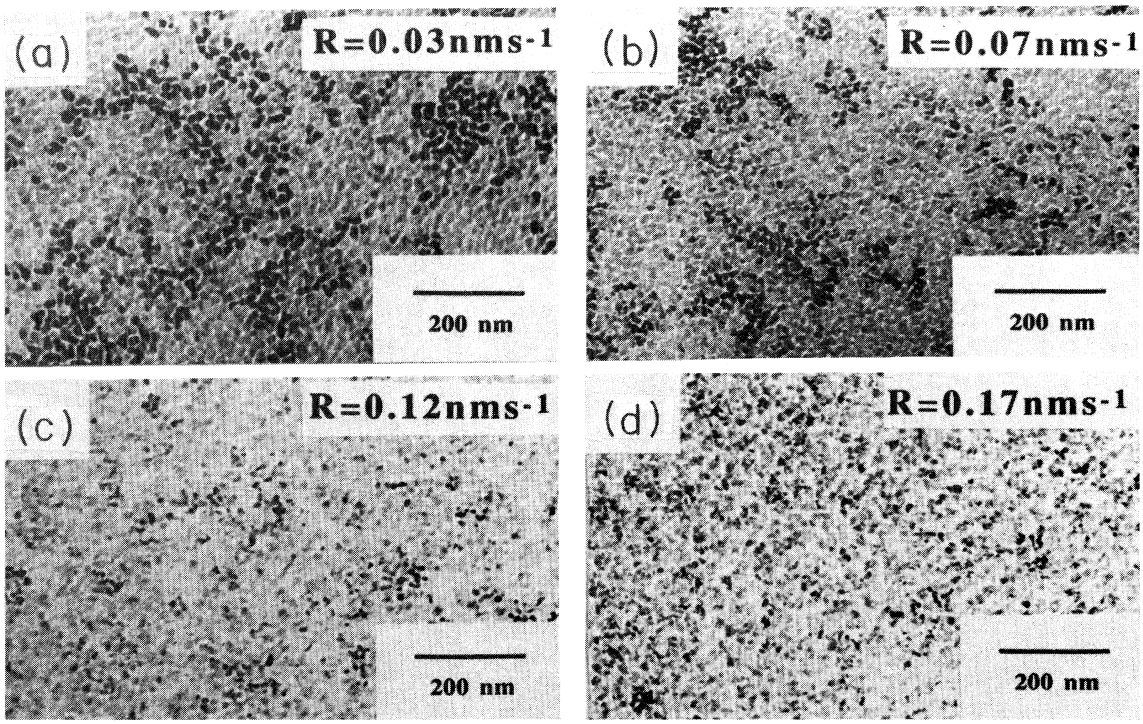


FIG. 3. TEM micrographs of 10-nm thick antimony deposits obtained by the LECBD technique with increasing deposition rate: (a) $R = 3\times10^{-2}$ nm s$^{-1}$, (b) $R = 7\times10^{-2}$ nm s$^{-1}$, (c) $R = 1.2\times10^{-1}$ nm s$^{-1}$, and (d) $R = 1.7\times10^{-1}$ nm s$^{-1}$. The mean size of incident clusters is about 36 atoms.

nm. The size of grains forming the film decreases with increasing deposition rate. At a low value of $R$ [Fig. 3(a)], the size of supported particles is 14.5 nm in diameter. This diameter ($D$) decreases to 8 nm, when $R$ increases up to $1.7\times10^{-1}$ nm s$^{-1}$, and corresponds nearly to the thickness of the deposit. The percolation threshold is always reached in the range of the deposition rate studied in this work.

### C. Percolation threshold study

In the case of antimony deposited by MBD, a crystalline and continuous film can be obtained if the deposit is thick enough. Typical transmission electron micrographs showing the coverage rate evolution are presented on Fig. 4. For a $3\times10^{-2}$ nm s$^{-1}$ deposition rate, the percolation threshold is reached for a 20-nm-thick deposit [Fig. 4(c)]. For lower thicknesses [Figs. 4(a) and 4(b)], Sb deposits present separate amorphous particles.

For Sb deposits obtained by LECBD, the coverage rate (or percolation threshold) depends on the incident cluster size as illustrated in Fig. 2. In the thickness range (1–5 nm), the percolation threshold appears at lower thickness when the incident cluster size increases. We have also found that the percolation threshold is about 3 nm for incident cluster of 240 atoms and about 5 nm for incident clusters of 36 atoms. The influence of the deposition rate has also been observed, in our experiments, on the percolation threshold indicating that the percolation threshold is reached for lower thickness when the deposition rate increases.

### D. Crystallographic structure

As previously mentioned,[11] antimony deposits are amorphous and discontinuous in the first stage of MBD deposition. Antimony crystallizes above a critical thickness $d_c$, depending on the nature, temperature and preparation of the substrate (Fig. 5). Under the conditions used in our experiments, the value of $d_c$ is about 20 nm for the Sb/$a$-C system. The value that we obtained (Fig. 5, $d_c=7$ nm) is different from that obtained by Hashimoto.[12] This difference can be explained by the fact that the deposition rate in Hashimoto's experiments was ten times higher than the one used in our experimental procedure.

The diffraction patterns obtained for Sb deposited by LECBD [for instance, the ones corresponding to micrographs of Figs. 3(a)–3(d)] have been indexed with the well-known $\alpha$-Sb structure. Nevertheless, it can be pointed out that, for the two lower deposition rate specimens [Figs. 3(a) and 3(b)], the nearly continuous layer is formed with large areas of crystalline metallic islands (the diameter of the area is about 100–200 nm) in which supported particles present the same crystallographic orientation. At a higher value of $R$ [Figs. 3(c) and 3(d)], the structure of the deposit is more polycrystalline and no such areas have been observed. Moreover, this phenomenon can be observed with an increase of the incident cluster size.

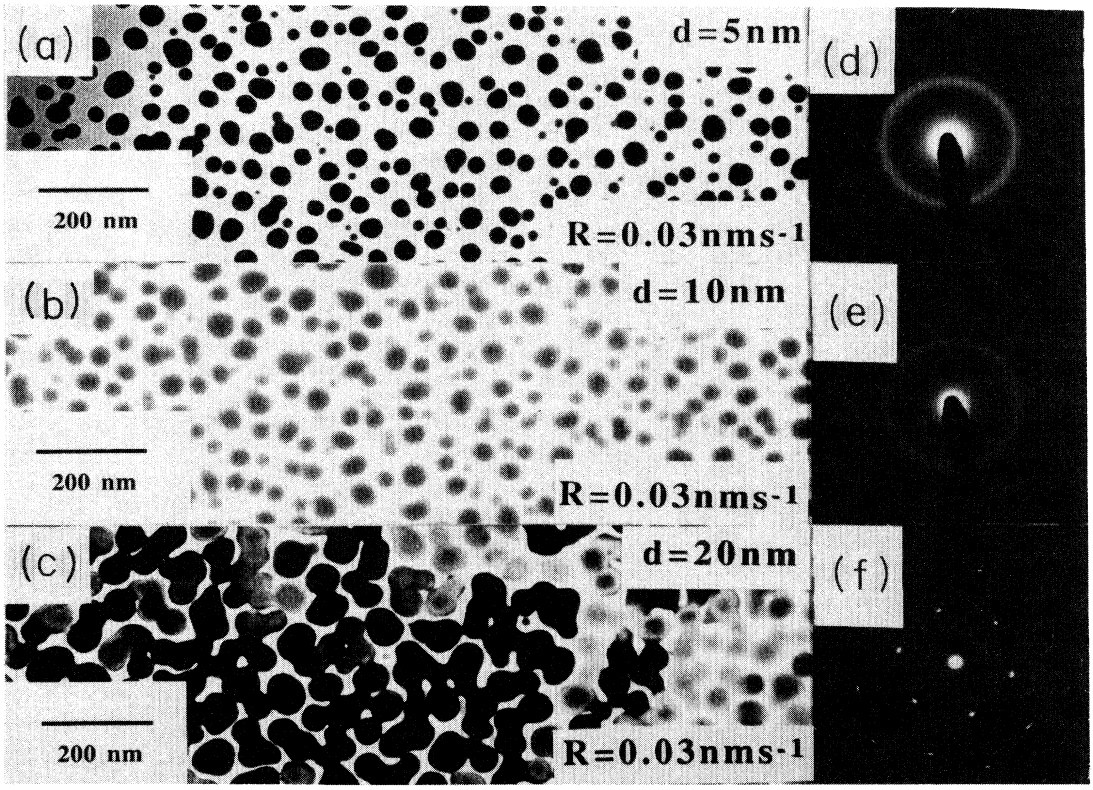


FIG. 4. (a)–(c) TEM micrographs and (d)–(f) the corresponding diffraction patterns of antimony deposits obtained by the MBD technique for increasing thickness of deposits: (a) $e=5$ nm, (b) 10 nm, (c) 20 nm. The deposition rate is $R=3\times10^{-2}$ nm s$^{-1}$.

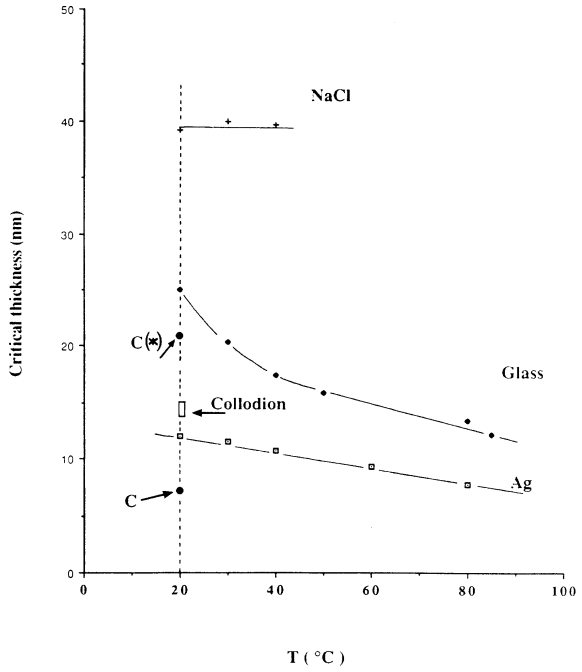


FIG. 5. Evolution of the critical thickness vs nature and temperature of substrate in the case of antimony MBD. The critical thickness obtained in this work is labeled (*). Results obtained on NaCl, glass, collodion, silver, and carbon have been obtained, respectively, in Refs. 28, 29, 12, 30, and 12. The deposition rates are $R=3$ nm s$^{-1}$ for NaCl and for glass, $R=0.3$ nm s$^{-1}$ for C and for collodion, $R=0.1$ nm s$^{-1}$ for Ag, and $R=0.03$ nm s$^{-1}$ for C (*).

Large single-crystalline domain areas are observed with small incident clusters (up to 48 atoms), whereas large incident clusters (240 atoms) give a polycrystalline film.

The relation between the amorphous-crystal transition and the percolation threshold has been invoked but never explained. For MBD and LECBD, the deposits are always amorphous before the percolation threshold. The stability of the amorphous phase has been explained by Palatnik *et al.*[13] Among the isolated amorphous particles, a few crystallized particles have been detected recently by HRTEM (high-resolution transmission electron microscopy) observations and are expected to be the crystallization nuclei beyond the percolation threshold.[14]

## IV. DISCUSSION

### A. Growth models

To help us interpret our experimental results on thin metallic antimony films, the onset of the growth has been investigated. At low coverage, dynamic or static coalescence are very low and allow us to study the nucleation growth stages.[15] The problem involved in the interpretation of nucleation data is to entirely define the experimental system and to control the parameters (geometry, electronic structure, and chemical composition of the surface, etc.,). Our experimental data are reproducible but "uncontrolled." However, the growth behavior can be qualitatively discussed from the classical statistic model of nucleation.

The nucleation rate $J$ for small nuclei can be expressed using a statistic model[16]

$$J=NR\langle a\rangle^2(R/\nu N)^{n^*-1} \times\exp[(n^*E_{\rm ad}+E_{n^*-1}-E_{\rm SD})/kT] , \quad (1)$$

where $n^*$ is the number of atoms in the smallest stable cluster, $R$ is the impinging vapor flux, $N$ is the number density of adsorptions sites on the surface, $\nu$ is the frequency of vibration, $E_{\rm ad}$ is the binding energy of the elementary particle ($Sb_4$ or incident cluster in our case) to a perfect surface, $E_{n^*}$ is the dissociation energy of the critical nuclei, $E_{\rm SD}$ is the activation energy for surface diffusion, and $\langle a\rangle$ is the mean distance covered in a single jump. For the nucleation occurring at preferential sites $J=J_{\rm PS}$. The validity of Eq. (1) has been discussed elsewhere.[17,18] The qualitative approach gives $n^*=1$ and $N=N_0$ ($N_0$ is the number density of preferential sites). [The critical value $n^*$ is not well defined. Assuming that $Sb_4$ is an elementary particle, the critical size corresponds to the quasidimer $Sb_4$-$Sb_4$ and $n^*=2$. On the other hand, tetramer is expected to be greater than the critical nuclei ($Sb_2$) and Gibb's barrier corresponds to the elementary particle which gives $n^*=1$.]

The dependence of the cluster density versus time is given[19–21] by the classical rate equation for complete condensation when reevaporation is not significant,

$$(N_x=\alpha D_i^{-1/3}t^{1/3}) , \quad (2)$$

and for incomplete condensation when reevaporation controls the adatom (elementary particle) population

$$N_x=\beta D_i t . \quad (3)$$

$\alpha$ and $\beta$ are adjustable parameters and $D_i$ is the diffusion coefficient of the incident particle (the adatom in the classical configuration). Qualitatively, the dependence of $N_x$ and $J$ versus the deposition rate $R$ (the temperature effect has not been investigated) is in good agreement with our experiments for $Sb_4$ and cluster depositions. A more in-depth analysis will be discussed now.

### B. Growth mechanism of antimony deposited by MBD

#### 1. Nucleation data

In our experiments, the time dependence of the stable particle density has been found experimentally to be

$$N_x \propto t^{0.82\pm0.05} . \quad (4)$$

The saturation number $N_s$ is about $1.6\times10^{10}$ cm$^2$. The experimental law corresponds to the onset of the nucleation with a low coverage (<5%). The experimental sticking coefficient of $Sb_4$ varies from 33 to 56% and increases with the coverage rate. The prediction of incomplete condensation seems to be reasonable. The law dependence is in agreement with Eq. (3). The nucleation rate $J$ [$J=(\partial N_x/\partial t)_{t=0}$] measured from the experimental

curve) is about $1.3\times10^{7}$ $cm^{-2}s^{1}$ ($T=300$ K, $R=1.7\times10^{13}$ atoms $cm^{-2}$). This value is 3 orders magnitude lower than the values obtained for other elements [In/$a$-C, $1.3\times10^{10}$ $cm^{-2}s^{-1}$; $Bi_2/a$-C, $7.7\times10^{10}$ $cm^{-2}s^{-1}$ (Ref. 22)]. This low value can be explained either by a preferential nucleation upon a low number of specific defects (which are the preferential sites) or a small value of the exponential factor in Eq. (1). Therefore, the interaction between $Sb_4$ and the substrate and the activation energy for surface diffusion must be weak. [The case corresponding to $E_{SD}$ closed to $E_{ad}$ is not taken into account. The activation energy $E_{SD}$ depends strongly on the substrate nature but its value is expected to be lower than a third of the adsorption energy $E_{ad}$. Some experimental data are given in Refs. 23 and 24.]

#### 2. *High mobility of supported particles*

The binding energy of antimony clusters is expected to vary on the substrate when the size of the supported antimony particle increases because the binding energy value of the *free* antimony cluster is a function of the cluster size. From $Sb_4$ to $Sb_{20}$, experimental results on the binding energy of $Sb_4$ units inside an antimony free cluster is 1.3 eV.[9] This value is well below the energy corresponding to the evaporation of $Sb_4$ in the bulk (2.1 eV).[4] This suggests that the clusters of antimony consist of weakly bonded packing of tetramers (see Fig. 1). This structure can be understood from the properties of column-VB elements (P, As, Sb). In particular, Pauling and Simonetta using quantum chemistry considerations have found that, in the $P_4$ tetramer, the bonding orbitals have 98% of $p$ character, the remaining 2% sharing between $s$ or $d$ character. ($P_8$ must be weakly bonded because the three $p$ electrons of each atom give covalent bonds in tetrahedral symmetry.) No calculation has been made on $Sb_{4n}$ clusters but we can try to understand the difference between the binding energy of $Sb_{4n}$ clusters relative to the evaporation of $Sb_4$. For Sb clusters, the percentage of the 5-$s$ and 5-$d$ characters is slightly higher than 2%: hybridization and delocalization is more intense in antimony than in phosphorous (Sb has a more pronounced metallic character in the bulk than P and the 5-$s$ and 5-$d$ character bonds with larger orbital overlap can explain as well the tendency towards the formation of tetramers in antimony as the predominance of the cluster structures built from $Sb_4$ units. When the supported particle size increases, the binding energy increases from 1.3 to 2.1 eV and so the surface free enthalpy increases too. The metastable character of the $Sb_4$ packing structure suggests that a phase transition corresponding to $Sb_{4\,packing}\rightarrow Sb_{bulk}$ is reached for a critical size $n_c$ (corresponding to the $s$-$p$ hybridization in bulk). Below the critical size, the bond between the particle and the substrate is weak, whereas above the critical size the hybridization increases; therefore, the exponential factor in Eq. (1) must increase.

#### 3. *Evidence of specific defects*

Small clusters are difficult to trap on the standard adsorption $a$-C sites. The activation energy of the specific defects must be high. Hybridization between Sb and dangling bonds of an $a$-C site is a possible explanation. On silicon, which is also an element of the column IVB, a chemical bond has been evidenced between $Sb_4$ and Si.[25] Contamination by hydrocarbon molecules on the $a$-C surface in another explanation. Assuming a mean number density of standard adsorption sites for $Sb_4/a$-C of about $1.3\times10^{15}$ $cm^{-2}$ (each atom of the surface can be a nucleation center), the number of specific defects ($N_s=1.6\times10^{10}$ $cm^{-2}$) corresponds to a surface-defect concentration of 12 ppm, assuming one defect site on the surface per impurity atom.

### C. Growth mechanism of antimony deposited by LECBD

#### 1. *Nucleation data*

For the LECBD experiments performed with a cluster mean size of 36 atoms, the experimental time dependence of the stable particle density is found to be

$$N_x \propto t^{0.4\pm0.1} . \tag{5}$$

The sticking coefficient of the incident clusters has been found very close to unity, so this law is in favor of classical growth corresponding to Eq. (2). The saturation number $N_s$ is about $3.6\times10^{11}$ $cm^{-2}$, which is about 20 times greater than in MBD deposits. This value is close to the one obtained for bismuth deposition ($5\times10^{11}$, $8\times10^{11}$ $cm^{-2}$ for the $Bi_2$ and $Bi_{90}$ depositions on the $a$-C substrate).[26] For the $Sb_{36}$ deposition, the nucleation rate is $J=0.3\times10^{10}$ $cm^{-2}s^{-1}$ ($T=300$ K, $R=1.7\times10^{13}$ atoms $cm^{-2}$), which is in agreement with the value found for other elements (see Sec. IV B 1). Equation (5) is expected to remain valid for a cluster mean size greater than 36 atoms. For bigger incident clusters, this dependence should be almost the same as the one of Eq. (2) ($N_x \propto t^{0.33}$). The nucleation growth of particles on the substrate can be studied based on the hypothesis of the previous model. Each incident cluster is taken as an individual entity and the deposited particles are assumed to be mobile below a critical size $n_c$. This critical size is more quickly reached when the size of the incident cluster increases. Assuming that the strength of the bond between the particle and the substrate increases strongly beyond the critical size, the diffusion coefficient must decrease rapidly and particles overpassing the critical size can stop anywhere on the substrate without necessarily reaching a PS. These nonoccupied PS can act as nucleation centers for smaller clusters and, finally, the density of particles on the substrate $N_s$ is larger than in the MBD case.

#### 2. *Influence of the size of the incident cluster*

The dependence of the diffusion coefficient as a function of the particle size can be estimated from the evolution of the number of supported particles versus the incident cluster size (corresponding to the same time of deposition and the same deposition rate). The experimental empiric law is given by

$$N_s \propto \langle n \rangle^{0.25\pm0.05} \quad (16<\langle n \rangle<240 \text{ atoms}) . \tag{6}$$

TABLE II. Value of the $i$ coefficient in the empiric law $D_{\langle n\rangle}=D_1\langle n\rangle^{-i}$.

| $i$ | 0.33 | 1.67 | 2 | 1.5 | 0.75 |
|---|---|---|---|---|---|
| $\langle n\rangle$ | 250 | >6 | 3–6 | | 16–240 |
| Reference | 32 | 33 | 33 | 31 | this work |

Equations (2), (5), and (6) give the dependence of the diffusion coefficient with the size

$$D_{\langle n\rangle}=D_{\langle 16\rangle}\langle n/16\rangle^{-0.75}\ . \tag{7}$$

$D_{\langle 16\rangle}$ is relative to the cluster $Sb_{16}$, where $Sb_{16}$ is an elementary particle. This empiric law is in good agreement with the Kashchiev predictions ($D_{\langle n\rangle}=D_1\langle n\rangle^{-i}$, where $i$ is a constant coefficient.[27] Comparison with literature data is given in Table II. Assuming that the growth model is valid, the deposition of incident clusters is a direct method to estimate the diffusion coefficient of a cluster versus its size.

### D. Crystallographic structure of the thin film

As mentioned previously, small crystalline nuclei allow the crystallization of other particles. The number of these nuclei is probably proportional to the number of deposited particles. Therefore, above the percolation threshold, each nucleus induces crystallization of the supported particles located in its neighborhood. Finally, each domain has its own orientation on the substrate. Epitaxial growth allowing the formation of large domains in the same crystallographic orientation depends on three parameters: the activation energy for the formation of nuclei, the activation energy for the growth of the crystal, and the interfacial energy between two disordered domains required to obtain a single orientation. Epitaxial growth is more difficult if the initial number of disordered particles is large (the last contribution increases with the number of particles). In conclusion, the film tends to be formed with small crystalline particles in the case of LECBD deposition.

## V. CONCLUSION

From a technical point of view, it is important to obtain very thin and continuous films. In the case of antimony deposits on the $a$-C substrate, the LECBD technique is quite promising in comparison with the MBD technique. The difference in the growth mechanism between MBD and LECBD is attributed to the good sticking coefficient and the low diffusion on the substrate in the case of the big cluster deposition. The LECBD technique is a good method to estimate the dependence of the diffusion coefficient on the size of the particle. Moreover, an important advantage of the LECBD technique is that it allows control of the crystalline aspect of the deposit. For a given deposition rate, a beam of the small incident cluster will allow us to obtain deposits built with large supported particles presenting a preferential crystallographic orientation on large areas while a large incident cluster beam will produce polycrystalline films. It is noteworthy that, in both cases, the increase of the deposition rate tends to promote a continuous film with small supported particles presenting no preferential crystallographic orientation.

## ACKNOWLEDGMENTS

We are grateful to J. Richer for helpful discussion during this work.

[1]R. A. Metzger and F. G. Allen, Surf. Sci. **137**, 397 (1984).
[2]D. C. Streit, R. A. Metger, and F. G. Allen, Appl. Phys. Lett. **44**, 234 (1984).
[3]H. Siugura, J. Appl. Phys. **51**, 2630 (1980).
[4]G. M. Rosenblatt and P. K. Lee, J. Chem. Phys. **52**, 1454 (1970).
[5]G. Fuchs, M. Treilleux, F. Santos Aires, B. Cabaud, P. Melinon, and A. Hoareau, Phys. Rev. A **40**, 6128 (1989).
[6]F. Santos Aires, M. Treilleux, G. Fuchs, A. Hoareau, P. Melinon, and B. Cabaud, Z. Phys. **12**, 149 (1989).
[7]K. Sattler, J. Muhlbach, and E. Recknagel, Phys. Rev. Lett. **45**, 821 (1980).
[8]P. Melinon, Ph.D. thesis, University of Lyon, 1986.
[9]D. Rayane, P. Melinon, B. Tribollet, B. Cabaud, A. Hoareau, and M. Broyer, J. Chem. Phys. **91**, 3100 (1989).
[10]M. Broyer, B. Cabaud, A. Hoareau, P. Melinon, D. Rayane, and B. Tribollet, Mol. Phys. **62**, 559 (1987).
[11]H. Levinstein, J. Appl. Phys. **20**, 306 (1949).
[12]M. Hashimoto, M. Itoh, H. Kuromachi, and J. Takei, Thin Solid Films **161**, 123 (1988).
[13]L. S. Paltnik and V. M. Kosevich, Kristallografiya **3**, 709 (1958) [Sov. Phys. Crystallogr. **3**, 716 (1960)].
[14]G. Fuchs, M. Treilleux, F. Santos Aires, B. Cabaud, P. Melinon, and A. Hoareau, Thin Solid Films (to be published).
[15]G. A. Efendiev and F. I. Aliev, Dokl. Akod. Nauk SSSR **179**, 314 (1968) [Sov. Phys. Dok. **13**, 220 (1968)].
[16]D. Walton, J. Chem. Phys. **10**, 2182 (1962).
[17]A. Grant Elliot, Surf. Sci. **44**, 337 (1974).
[18]J. L. Robins and T. N. Rhodin, Surf. Sci. **2**, 346 (1964).
[19]G. Zinmeister, Thin Solid Film **2**, 497 (1968).
[20]D. R. Frankl and J. A. Venables, Adv. Phys. **19**, 409 (1970).
[21]J. A. Venables, Philos. Mag. **27**, 697 (1973).
[22]F. Santos Aires, Ph.D. thesis, University of Lyon, 1990.
[23]J. A. Venables, G.D.T. Spiller, and M. Hanbucken, Rep. Prog. Phys. **47**, 399 (1984).
[24]H. Poppa, J. Vac. Sci. Technol. **2**, 42 (1965).
[25]S. Andrieu, Surf. Sci. **219**, 277 (1989).
[26]F. Santos Aires, M. Treilleux, G. Fuchs, A. Hoareau, P. Melinon, and B. Cabaud, Z. Phys. D **12**, 149 (1989).
[27]D. Kashchiev, Surf. Sci. **55**, 477 (1976).

[28]M. Hashimoto, Jpn. J. Appl. Phys. **21**, 1099 (1982).
[29]M. Hashimoto, H. Niizeki, and K. Kambe, Jpn. J. Appl. Phys. **19**, 21 (1980).
[30]M. Hashimoto and K. Kambe, Thin Solid Films **94**, 185 (1982).
[31]K. Kinosita, Thin Solid Films **85**, 223 (1981).
[32]D. Kashchiev, Surf. Sci. **55**, 477 (1976).
[33]B. Lewis, Surf. Sci. **21**, 289 (1970).

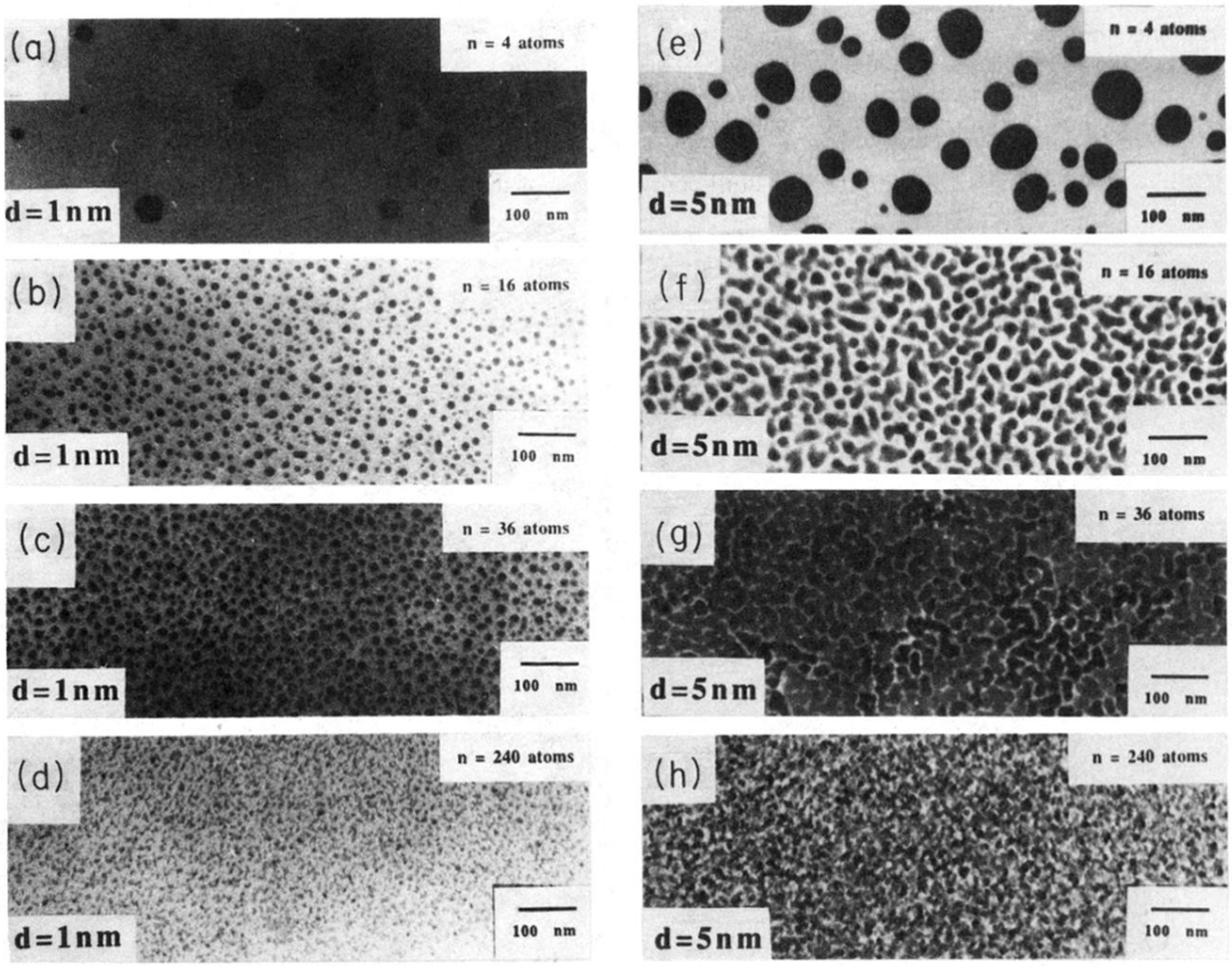


FIG. 2. TEM micrographs of 1-nm- (a)–(d) and 5-nm-thick antimony deposits (e)–(h) obtained with increasing incident mean cluster size: (a) and (e) $N=4$ atoms (MBD), (b) and (f) $N=16$ atoms, (c) and (g) $N=36$ atoms, and (d) and (h) $N=240$ atoms. The deposition rate is fixed at $5\times10^{-3}$ nm s$^{-1}$.

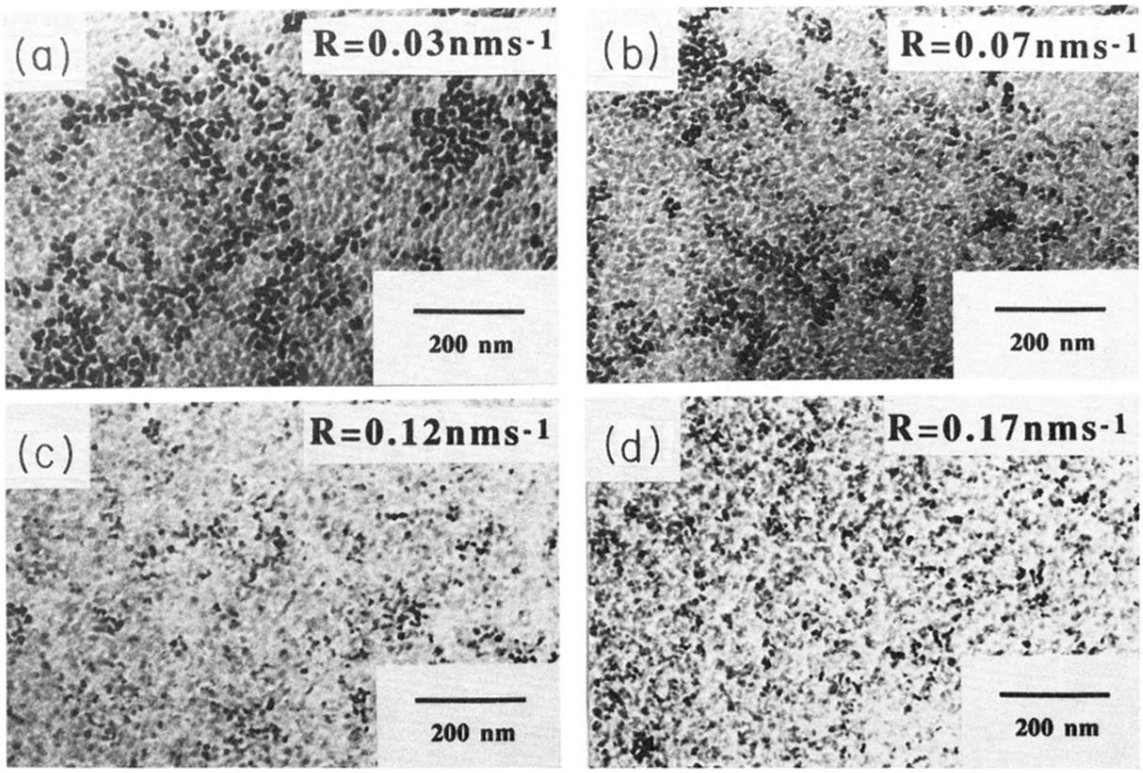


FIG. 3. TEM micrographs of 10-nm thick antimony deposits obtained by the LECBD technique with increasing deposition rate: (a) $R = 3 \times 10^{-2}$ nm s$^{-1}$, (b) $R = 7 \times 10^{-2}$ nm s$^{-1}$, (c) $R = 1.2 \times 10^{-1}$ nm s$^{-1}$, and (d) $R = 1.7 \times 10^{-1}$ nm s$^{-1}$. The mean size of incident clusters is about 36 atoms.

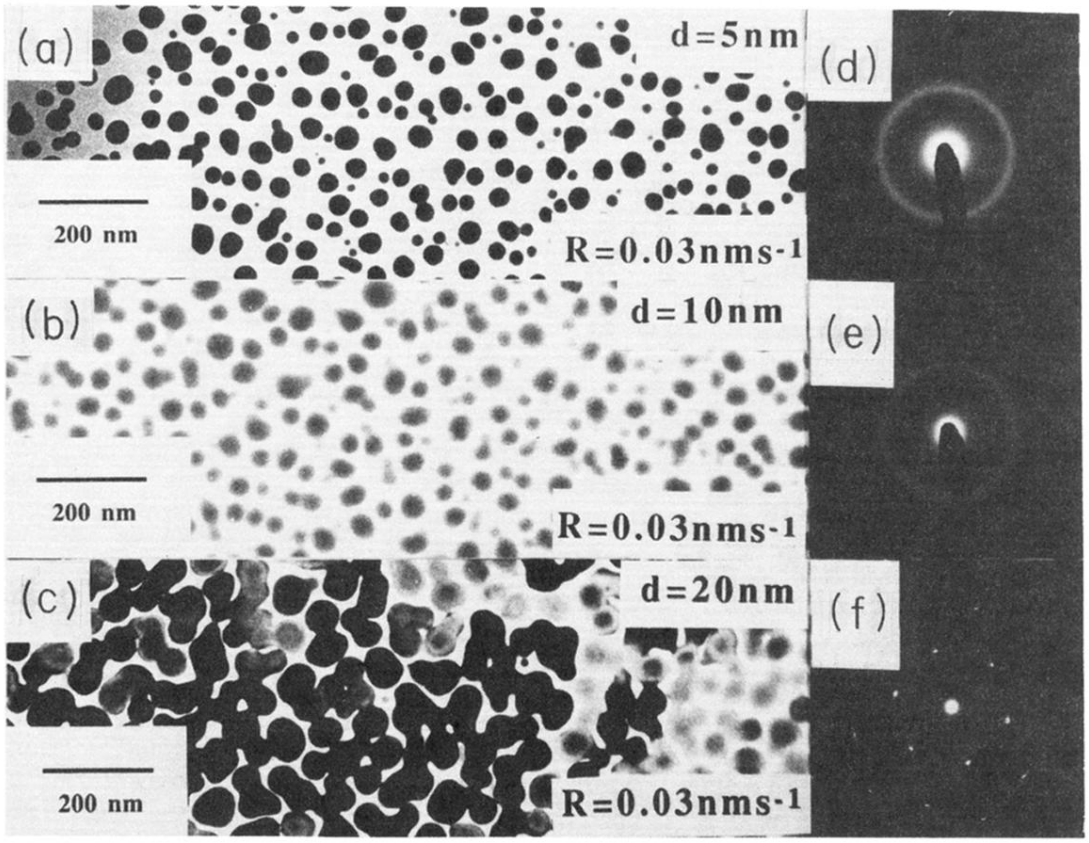


FIG. 4. (a)–(c) TEM micrographs and (d)–(f) the corresponding diffraction patterns of antimony deposits obtained by the MBD technique for increasing thickness of deposits: (a) $e = 5$ nm, (b) 10 nm, (c) 20 nm. The deposition rate is $R = 3 \times 10^{-2}$ nm s$^{-1}$.